J_{eff} Description of the Honeycomb Mott Insulator α-RuCl$_3$

A. Koitzsch,[1] C. Habenicht,[1] E. Müller,[1] M. Knupfer,[1] B. Büchner,[1,2] H. C. Kandpal,[1,3]
J. van den Brink,[1,4] D. Nowak,[5] A. Isaeva,[5] and Th. Doert[5]

[1]*IFW-Dresden, P.O.Box 270116, D-01171 Dresden, Germany*
[2]*Institute for Solid State Physics, TU Dresden, D-01062 Dresden, Germany*
[3]*Indian Institute of Technology, Department of Chemistry, Roorkee 247 667, India*
[4]*Institute for Theoretical Physics, TU Dresden, D-01062 Dresden, Germany*
[5]*Department of Chemistry and Food Chemistry, TU Dresden, D-01062 Dresden, Germany*

Novel ground states might be realized in honeycomb lattices with strong spin-orbit coupling. Here we study the electronic structure of α-RuCl$_3$, in which the Ru ions are in a d^5 configuration and form a honeycomb lattice, by angle-resolved photoemission, x-ray photoemission, and electron energy loss spectroscopy supported by density functional theory and multiplet calculations. We find that α-RuCl$_3$ is a Mott insulator with significant spin-orbit coupling, whose low energy electronic structure is naturally mapped onto J_{eff} states. This makes α-RuCl$_3$ a promising candidate for the realization of Kitaev physics. Relevant electronic parameters such as the Hubbard energy U, the crystal field splitting 10 Dq, and the charge transfer energy Δ are evaluated.

The search for novel electronic and magnetic ground states has ever been a driving force of condensed matter physics. The effects of strong spin-orbit coupling, possibly competing with other energy scales, have turned out to be especially fruitful in this respect in recent years. This is most prominently manifested by the advent of topological insulators [1]. More recently, the Kitaev model was established, which describes the bond-dependent spin interactions on a honeycomb spin 1/2 lattice [2]. The Kitaev model attracts enormous attention because it is exactly solvable and its ground state is an exotic quantum spin liquid. However, unambiguous experimental evidence is lacking so far. The prime candidates for the realization of Kitaev physics have been the $5d^5$ iridates A_2IrO$_3$ (A = Na, Li) [3–7]. This thread of research relies on the realization of effective $J_{\text{eff}} = 1/2$ pseudospins by the combined interaction of spin-orbit coupling and crystal field splitting. But the concept of $J_{\text{eff}} = 1/2$ pseudospins is under debate for the iridates due to substantial lattice distortions lifting the t_{2g} degeneracy, which, strictly speaking, invalidates the J_{eff} description.

α-RuCl$_3$ appeared recently against this background as a $4d$ analogue to the iridates [8,9]. Ru is in a $3+$ state and features a d^5 electron count with a low spin state. Its spin-orbit coupling ($\lambda \approx 0.1$ eV) is strongly reduced as compared to the iridates, but so is its bandwidth W due to presumed correlation effects. Importantly, the local cubic symmetry is almost perfect in contrast to the iridates. Hence, the J_{eff} description might be still operable for α-RuCl$_3$. Another practical advantage is that it can be synthesized as large, easy-to-cleave single crystals, which offer the possibility of exfoliation.

RuCl$_3$ has been known for a long time and is even of some importance as a chemical [10]. Its electronic structure has been repeatedly investigated over the years by optical spectroscopy and photoemission [11–13]. The picture of a Mott-insulating state was proposed where the Ru $4d$ bands are situated close to E_F but show little dispersion [13]. More recent optical data confirmed the magnitude of the charge gap $E_G \approx 1.1$ eV, which is much smaller than the charge transfer energy $\Delta \approx 5$ eV as expected for a Mott insulator [14]. U has been estimated to be about 1.5 eV [8,13,15], a value often used as an input parameter for band structure calculations.

As for the magnetic properties, one or two (depending on the study) phase transitions at $T \approx 7$ and 15 K are reported [16–19]. A strong magnetic anisotropy is found with large effective moments exceeding the $S = 1/2$ limit and implying a large orbital contribution. Neutron scattering below $T = 7$ K is consistent with a zigzag type order, one of the types of magnetic order predicted within the framework of the Kitaev-Heisenberg model [9,15,18–20].

Here we elucidate the electronic structure of α-RuCl$_3$ by state of the art photoemission (PES), electron-energy-loss spectroscopy (EELS), density-functional-theory (DFT), and multiplet calculations. We achieve a consistent, quantitative picture of a spin-orbit assisted Mott insulator. The central question of this study, and decisive for the prospects of α-RuCl$_3$ as a possible carrier of Kitaev ground states, is whether or not the $J_{\text{eff}} = 1/2$ description of the electronic structure is appropriate. Based on the comparison of the DFT calculations with results from angle-resolved photoemission spectroscopy (ARPES), we can answer this question affirmatively.
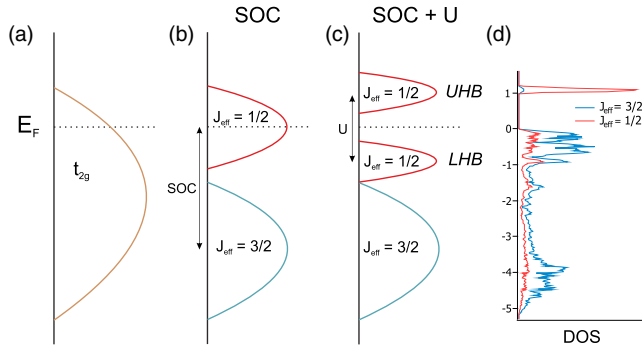
FIG. 1.   (a)–(c) J_{eff} description of the d-level electronic structure. (a) Schematic density of states without interactions. (b) Under the presence of strong spin-orbit coupling. (c) With spin-orbit coupling and on-site correlation U. (d) Calculated density of states of α-RuCl$_3$ with spin-orbit coupling and on-site correlation.

FIG. 2.   Valence band of α-RuCl$_3$ measured by photoemission spectroscopy with different photon energies at room temperature compared to an orbital projected density of states calculation.

Platelet-like single crystals up to several mm in diameter of α-RuCl$_3$ were grown by chemical vapor transport reactions. PES measurements were performed using a laboratory based system at room temperature after cleaving the crystals *in situ*. The EELS (Electron Energy Loss Spectroscopy) measurements in transmission have been conducted using thin films ($d \approx 100$ nm) at $T = 20$ K. The density functional calculations were performed using the all-electron full-potential local-orbital (FPLO) code [21,22] within Perdew-Wang parametrization [23]. See the Supplemental Material for details [24].

Under a cubic crystal field, the $4d$ electron manifold of Ru splits into t_{2g} and e_g states separated by the crystal field splitting parameter 10 Dq. Figure 1(a) shows schematically the t_{2g} states. This band cuts the Fermi energy (E_F), because in a low-spin configuration with 5 d-delectrons it is not completely filled. Introducing the spin-orbit coupling, the $J_{\mathrm{eff}} = 1/2$ and $3/2$ states separate from each other [Fig. 1(b)]. The on-site correlation energy U causes a gap opening within the $J_{\mathrm{eff}} = 1/2$ band. Figure 1(d) shows the density of states (DOS) of α-RuCl$_3$ obtained by DFT calculated by taking into account spin-orbit coupling (SOC) and the correlation energy ($U = 2$ eV, $J_H = 0.4$ eV, $U_{\mathrm{eff}} = 1.6$ eV) projected onto $J_{\mathrm{eff}} = 1/2$ and $3/2$. The DOS correctly reproduces the gap opening and the insulating nature of α-RuCl$_3$. Comparing it to the general J_{eff} picture, it bears out the almost pure $J_{\mathrm{eff}} = 1/2$ character of the sharp upper Hubbard band (UHB). The lower Hubbard band (LHB), on the other hand, is strongly mixed with the $J_{\mathrm{eff}} = 3/2$ states. This is a consequence of the antiferromagnetic order imposed on this calculation, which gives the lowest total energy. The J_{eff} description appears to be well justified by the DFT in agreement with previous studies [15,18]. In the following we compare the DFT to a variety of experimental probes.

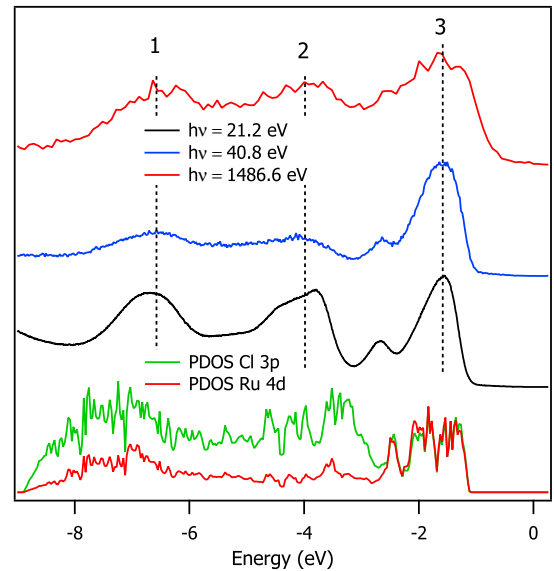Figure 2 shows angle-integrated photoemission spectra of the valence band region taken with three different photon energies. The spectra consist of three main features, labeled 1–3. Their relative intensity varies as a function of photon energy. Peaks 1 and 2 display an intensity minimum relative to peak 3 for $h\nu = 40.8$ eV. This reflects the different orbital character of the underlying states, which causes a different dependence of the photoionization cross section on photon energy. By comparison with tabulated values, peak 1 and 2 can be assigned to Cl $3p$ and peak 3 to the Ru $4d$ states [29] in agreement with previous results [12]. However, an important difference to the earlier studies is that we observe a larger gap. The onset of the valence band is located at $E_{\mathrm{VBO}} \approx 1$ eV. The data reported by a very recent ARPES study, on the other hand, are similar to our results [30]. Together with $E_G \approx 1.2$ eV (see Fig. 3) this places the Fermi level close to the bottom of the d^6 conduction band. The full width half maximum of the Ru $4d$ peak (without the shoulder at $E = -2.7$ eV) is $W_{4d} = 0.75$ eV only, which indicates that the system is susceptible to correlation effects even for moderate values of U.

The lower part of Fig. 2 presents the Ru $4d$ and Cl $3p$ orbital projected DOS. It is identical to the DOS in Fig. 1(d) but has been renormalized for better comparison with experiment (stretching factor 1.5, offset 1.1 eV). The low energy region is dominated by the Ru $4d$ weight while at higher energies Cl $3p$ dominates in agreement with experiment.

Figure 3(a) exhibits the angle dependence of the valence band approximately along $M - \Gamma - K$ (see the Supplemental Material [24] for details). The renormalized theoretical band structure is overlayed over the experimental data. Two regimes can be distinguished: the low-energy region of weakly dispersing Ru $4d$ states and at higher
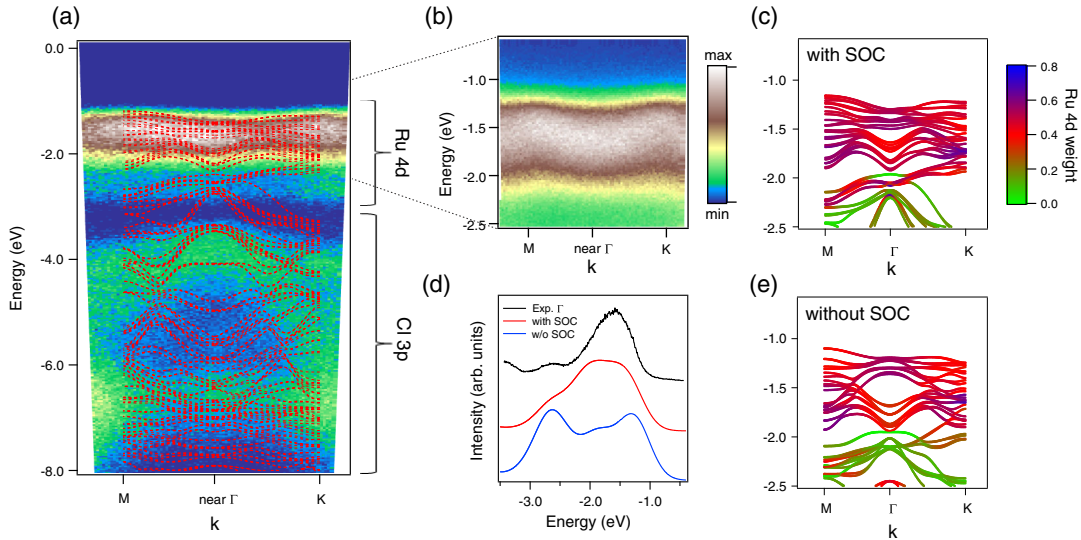
FIG. 3.   (a) Color coded representation of the angle dependence of the full valence band. Energy regions of mainly Ru $4d$ and Cl $3p$ character are denoted on the right side. Red dotted lines are results of band structure calculations under the same renormalization as the DOS in Fig. 2. (b) Expansion of the Ru $4d$ region. (c) Band structure without bandwidth renormalization but with offset. The color corresponds to the degree of Ru $4d$ orbital character. (d) Comparison of experimental and theoretical Γ-point spectra extracted from calculations with and without spin-orbit coupling (SOC). (e) Band structure without inclusion of the SOC.

energies more strongly dispersing Cl $3p$ derived bands, which are clearly separated from each other. The calculation is again in qualitative agreement to the data. The low-energy region is expanded in Fig. 3(b) along the same cut. The Ru $4d$ bands disperse on the order of 200 meV. They form a minimum around Γ and maxima around M and K. Note that this is not the dispersion of a single band, but a superposition of many d bands forming a broad peak. In order to compare it to theory, we present the unrenormalized, but offset low-energy band structure in Fig. 3(c). The total bandwidth and the principal shape of the dispersion approximately agree with experiment. In contrast, we show in Fig. 3(e) a calculation where the SOC has been switched off, that is, the J_{eff} mapping is not operable anymore. The shape of the Ru $4d$ derived bands significantly changes around Γ and the agreement with experiment worsens. Figure 3(d) compares experimental and theoretical Γ-point spectra. The latter have been extracted from the data in Figs. 3(b), 3(c), and 3(e) by considering the Ru $4d$ band weight at Γ and applying appropriate energy broadening. The model spectrum including the SOC compares reasonably well to experiment on a qualitative level, while the spectrum without SOC fails to do so. The difference is not as pronounced for the K and M point (not shown). Nevertheless, Fig. 3 underlines the importance of the SOC for the electronic structure of α-RuCl$_3$. The SOC also affects the conduction band and the gap value (see the Supplemental Material [24] for details).

The electronic structure of α-RuCl$_3$ bears out similarities to the iridates, e.g., Na$_2$IrO$_3$. In both cases there is a relatively broad, weakly dispersing t_{2g} band followed by

Cl/O-p bands at higher energies and a Mott-type gap [31]. The broadness of the d states has been explained in this case by the hampered hole motion in a Heisenberg-Kitaev spin background [32] or by polaronic effects [31,33].

The photoemission experiments presented so far probe the occupied states only. The charge gap is not accessible in this way. We have, therefore, performed EELS experiments and measured the loss function, which can be expressed as Im($-1/\epsilon$), where ϵ is the dielectric function (see Fig. 4). We assign peak A at $E_G = 1.2$ eV to interband transitions across the charge gap, i.e., $d^5 d^5 \rightarrow d^4 d^6$. This peak is rather sharp ($W_A = 0.3$ eV). Conventionally, one would relate E_G to U_{eff} and the onset of the gap feature with $U_{\mathrm{eff}} - \frac{1}{2} W_{\mathrm{LHB}} - \frac{1}{2} W_{\mathrm{UHB}}$. However, here the gap feature is narrower than the valence band alone, invalidating this view in its pure form. We propose instead that excitonic effects contribute to the gap excitation, which shifts spectral weight towards the low energy onset. Therefore, $E_G = 1.2$ eV should be considered as a lower boundary of U_{eff}.

Excitation B centered at $E = 2.1$ eV can be associated with the cubic crystal field splitting, i.e., excitations into the e_g states and is approximately 10 Dq. This claim will be substantiated further when discussing the core levels (Fig. 5). Features C and D are both due to Cl $3p$-Ru $4d$ charge transfer excitations. The onset of C is ≈ 3 eV which corresponds to the onset of peak 2 in Fig. 2. The energy scales of photoemission and energy loss agree roughly in this case because the d^6 conduction band is situated close to E_F. The energy difference of features C and D is equal to the separation of peaks 1 and 2 in Fig. 2, lending further support to this assignment. Both features are broad and
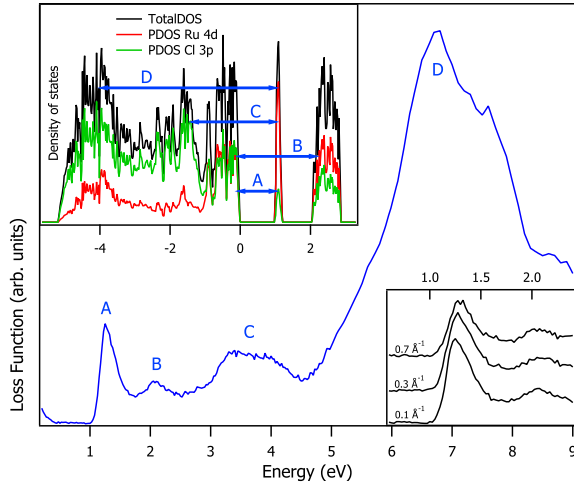
FIG. 4.   Loss function measured by EELS at $\mathbf{q} = 0.1$ Å. Lower inset: Low energy loss function as a function of momentum transfer. Upper inset: Orbital projected DOS with transitions labeled according to the peaks in the main panel.

FIG. 5.   Ru $3p$ EELS and XPS. Red lines show charge-transfer multiplet calculations (see text for details).

show fine structures reflecting the pronounced dispersion of the Cl $3p$ bands.

The lower inset of Fig. 4 shows the momentum dependence of the loss function. The overall dispersion of the gap excitation is small (≈ 50 meV). This is consistent with the valence band and conduction band dispersion being small. Comparing the DFT results for the conduction band dispersion with and without SOC the bandwidth increases by a factor of 2 for the latter, which is against the trend seen in the EELS momentum dependence (see Supplemental Material [24] for details). The upper inset shows again the DOS with an assignment of the transitions A–D.

Taking together Figs. 2–4, a consistent description of the electronic structure of α-RuCl$_3$ is obtained. The electronic parameters introduced so far (U, Δ, 10 Dq) determine the shape of the core levels, which can then be used to check the validity of the above arguments.

Figure 5 presents the $3p$ spectra measured by XPS (x-ray photoemission spectroscopy) and EELS, along with multiplet calculations using a joined set of parameters. The spectra are split due to the $3p$ spin-orbit interaction by 22 eV in a $3p_{3/2}$ and a $3p_{1/2}$ state. A double peak structure is observed in the EELS $3p_{3/2}$ line which is absent in $3p_{1/2}$ and in XPS. In fact, this double feature is a consequence of the spin-orbit coupling of the d electrons. The latter splits the d levels into $4d_{5/2}$ and $4d_{3/2}$ states. According to the J selection rule, the $4d_{3/2}$ state can be reached by both $3p_{1/2}$ and $3p_{3/2}$, whereas the $4d_{5/2}$ is accessible for the $3p_{3/2}$ state only. The double peak of the $3p_{3/2}$ EELS line indicates that the t_{2g} hole is of $J = 5/2$ character. The energy difference between the two components is mainly determined by the crystal field splitting.

For the photoemission, the transitions to t_{2g} or e_g are not operative and only one ionization peak is observed.
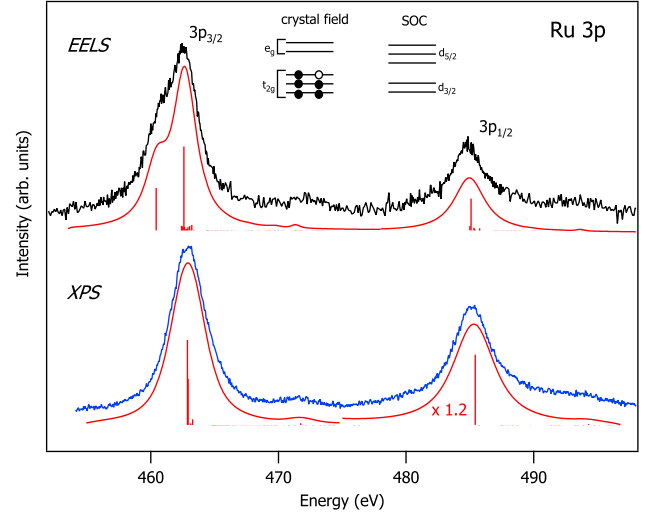
Figure 5 confirms that the spin-orbit coupling must be taken into account when describing the d electrons. A similar conclusion was drawn previously from the line shape of the Ru $L_{2,3}$ edge of x-ray absorption spectra [8].

Closer inspection reveals weak satellite features at the high energy side of the main peaks with an energy separation of about 8 eV. They originate from charge transfer processes, where an electron from the surrounding Cl ligands hops to the central Ru. We modeled the spectra by charge-transfer multiplet calculations using the CTM4XAS package [34]. Motivated by the low energy PES and EELS results discussed above, we fixed 10 Dq $= 2.2$, $\Delta = 5$ eV. The latter is to be considered as an average value for the broad energy region of charge transfer excitations seen in Fig. 4. The Slater integrals have been reduced to 25% of their atomic values [35]. We set the overlap integrals $T_{e_g} = 2$ eV and $T_{t_{2g}} = 1$ eV and the d-level core-hole repulsion $U_{dc} = 3$ eV. U_{dc} is always larger than U due to the more localized character of the core hole. With these parameters and appropriate Gaussian and Lorentzian broadening the red spectra are obtained. For XPS, quantitative agreement is accomplished. The branching ratio differs slightly, probably due to cross section and diffraction effects. The shape of the EELS spectrum is also correctly reproduced, in particular the line splitting of the $p_{3/2}$ peak. The satellite intensity is underestimated by the calculation due to the presence of a Ru $3p \rightarrow$ Ru $5s$ transition [36]. See the Supplemental Material for further XPS results [37].

In summary, we have investigated the electronic structure of α-RuCl$_3$ in detail. The photoemission data show a main Ru $4d$ contribution to the valence band at $E = -1.6$ eV with a width of $W_{4d} = 0.75$ eV and ≈ 200 meV dispersion. The data are well described by DFT calculations exhibiting a clear correspondence to the generic J_{eff}

description of local cubic systems with large spin-orbit coupling. From EELS measurements the direct gap is $E_g = 1.2$ eV with a sharp but weakly dispersing gap excitation mode. The electronic parameters obtained ($U_{eff} = 1.6$, $10 Dq = 2.2$, $\Delta = 5$ eV) are also successfully used for quantitative modeling of the EELS and photoemission core levels. The splitting of the $3p_{3/2}$ line into two components seen in EELS but not in XPS indicates the relevance of the SOC for the $4d$ electrons. The above observations convey the picture of a Mott insulator whose low-energy structure is dictated by a mixture of the local cubic symmetry and spin-orbit coupling which might give rise to exotic magnetic ground states.

[1] M. Z. Hasan and C. L. Kane, Rev. Mod. Phys. **82**, 3045 (2010).

[2] A. Kitaev, Ann. Phys. (Amsterdam) **321**, 2 (2006).

[3] J. Chaloupka, G. Jackeli, and G. Khaliullin, Phys. Rev. Lett. **105**, 027204 (2010).

[4] B. J. Kim, H. Jin, S. J. Moon, J.-Y. Kim, B.-G. Park, C. S. Leem, J. Yu, T. W. Noh, C. Kim, S.-J. Oh, J.-H. Park, V. Durairaj, G. Cao, and E. Rotenberg, Phys. Rev. Lett. **101**, 076402 (2008).

[5] Y. Singh and P. Gegenwart, Phys. Rev. B **82**, 064412 (2010).

[6] X. Liu, T. Berlijn, W.-G. Yin, W. Ku, A. Tsvelik, Y.-J. Kim, H. Gretarsson, Y. Singh, P. Gegenwart, and J. P. Hill, Phys. Rev. B **83**, 220403 (2011).

[7] S. K. Choi, R. Coldea, A. N. Kolmogorov, T. Lancaster, I. I. Mazin, S. J. Blundell, P. G. Radaelli, Y. Singh, P. Gegenwart, K. R. Choi, S.-W. Cheong, P. J. Baker, C. Stock, and J. Taylor, Phys. Rev. Lett. **108**, 127204 (2012).

[8] K. W. Plumb, J. P. Clancy, L. J. Sandilands, V. V. Shankar, Y. F. Hu, K. S. Burch, H.-Y. Kee, and Y.-J. Kim, Phys. Rev. B **90**, 041112 (2014).

[9] A. Banerjee, C. A. Bridges, J. Yan, A. A. Aczel, L. Li, M. B. Stone, G. E. Granroth, M. D. Lumsden, Y. Yiu, J. Knolle, D. L. Kovrizhin, S. Bhattacharjee, R. Moessner, D. A. Tennant, D. G. Mandrus, and S. E. Nagler, Nat. Mater. **15**, 733 (2016).

[10] D. M. Bose and H. G. Bhar, Z. Phys. **48**, 716 (1928).

[11] L. Binotto, I. Pollini, and G. Spinolo, Phys. Status Solidi B **44**, 245 (1971).

[12] I. Pollini, Phys. Rev. B **50**, 2095 (1994).

[13] I. Pollini, Phys. Rev. B **53**, 12769 (1996).

[14] L. J. Sandilands, Y. Tian, A. A. Reijnders, H.-S. Kim, K. W. Plumb, H.-Y. Kee, Y.-J. Kim, and K. S. Burch, Phys. Rev. B **93**, 075144 (2016).

[15] H.-S. Kim, V. Vijay Shankar, A. Catuneanu, and H.-Y. Kee, Phys. Rev. B **91**, 241110 (2015).

[16] M. Majumder, M. Schmidt, H. Rosner, A. A. Tsirlin, H. Yasuoka, and M. Baenitz, Phys. Rev. B **91**, 180401 (2015).

[17] J. A. Sears, M. Songvilay, K. W. Plumb, J. P. Clancy, Y. Qiu, Y. Zhao, D. Parshall, and Y.-J. Kim, Phys. Rev. B **91**, 144420 (2015).

[18] R. D. Johnson, S. C. Williams, A. A. Haghighirad, J. Singleton, V. Zapf, P. Manuel, I. I. Mazin, Y. Li, H. O. Jeschke, R. Valentí, and R. Coldea, Phys. Rev. B **92**, 235119 (2015).

[19] H. B. Cao, A. Banerjee, J.-Q. Yan, C. A. Bridges, M. D. Lumsden, D. G. Mandrus, D. A. Tennant, B. C. Chakoumakos, and S. E. Nagler, Phys. Rev. B **93**, 134423 (2016).

[20] H.-S. Kim and H.-Y. Kee, Phys. Rev. B **93**, 155143 (2016).

[21] K. Koepernik and H. Eschrig, Phys. Rev. B **59**, 1743 (1999).

[22] http://www.FPLO.de.

[23] J. P. Perdew and Y. Wang, Phys. Rev. B **45**, 13244 (1992).

[24] See Supplemental Material at http://link.aps.org/supplemental/10.1103/PhysRevLett.117.126403 for detailed description of methods and further experimental and DFT results, which includes Refs. [25–28].

[25] K. H. Huneke and H. Schfer, Z. Anorg. Allg. Chem. **534**, 216 (1986).

[26] J. Fink, Adv. Electron. Electron Phys. **75**, 121 (1989).

[27] F. Roth, A. König, J. Fink, B. Büchner, and M. Knupfer, J. Electron Spectrosc. Relat. Phenom. **195**, 85 (2014).

[28] E. V. Stroganov and K. V. Ovchinnikov, Ser. Fiz. Khim. **12**, 152 (1957).

[29] J. Yeh and I. Lindau, At. Data Nucl. Data Tables **32**, 1 (1985).

[30] X. Zhou, H. Li, J. Waugh, S. Parham, H.-S. Kim, J. Sears, A. Gomes, H.-Y. Kee, Y.-J. Kim, and D. Dessau, arXiv:1603.02279.

[31] R. Comin, G. Levy, B. Ludbrook, Z.-H. Zhu, C. N. Veenstra, J. A. Rosen, Y. Singh, P. Gegenwart, D. Stricker, J. N. Hancock, D. van der Marel, I. S. Elfimov, and A. Damascelli, Phys. Rev. Lett. **109**, 266406 (2012).

[32] F. Trousselet, M. Berciu, A. M. Oleś, and P. Horsch, Phys. Rev. Lett. **111**, 037205 (2013).

[33] K. M. Shen, F. Ronning, D. H. Lu, W. S. Lee, N. J. C. Ingle, W. Meevasana, F. Baumberger, A. Damascelli, N. P. Armitage, L. L. Miller, Y. Kohsaka, M. Azuma, M. Takano, H. Takagi, and Z.-X. Shen, Phys. Rev. Lett. **93**, 267002 (2004).

[34] E. Stavitski and F. M. de Groot, Micron **41**, 687 (2010).

[35] F. M. F. de Groot, Z. W. Hu, M. F. Lopez, G. Kaindl, F. Guillot, and M. Tronc, J. Chem. Phys. **101**, 6570 (1994).

[36] T. K. Sham, J. Am. Chem. Soc. **105**, 2269 (1983).

[37] See Supplemental Material at http://link.aps.org/supplemental/10.1103/PhysRevLett.117.126403 for additional XPS characterization, which includes Ref. [38].

[38] D. J. Morgan, Surf. Interface Anal. **47**, 1072 (2015).